Direct borohydride oxidation: mechanism determination and design of alloy catalysts guided by density functional theory

Gholamreza Rostamikia and Michael J. Janik*

Received 1st June 2010, Accepted 2nd July 2010
DOI: 10.1039/c0ee00115e

Direct borohydride fuel cells (DBFCs) convert an aqueous soluble, high specific energy density borohydride fuel directly to electrical energy. The lack of effective anode electrocatalysts for the anodic oxidation of borohydride limits the efficiency and power density attainable in these devices. The complexity of the eight electron reaction makes experimental determination of the reaction mechanism extremely challenging, thereby hampering the development of a rationale for optimizing catalyst composition. Computational quantum mechanical methods provide a unique tool for evaluating elementary step reaction kinetics in this system, and can be applied to guide a rational catalyst design procedure. In this perspective, we review the experimental literature on borohydride oxidation catalysis and discuss the usefulness of quantum mechanical methods towards electrode design. Mechanistic insights provided by these computational methods are discussed as well as the prospects of applying a computationally guided design procedure towards developing novel catalyst compositions.

1. Introduction

Direct borohydride fuel cells (DBFCs) offer the potential for direct chemical to electrical energy conversion from a high specific energy, water soluble fuel. These alkaline fuel cells operate using a base-stabilized aqueous borohydride (ex. $NaBH_4$) solution as the anode fuel and oxygen or air at the cathode. The use of an aqueous sodium borohydride solution as an anode fuel for an alkaline fuel cell was initially reported in the 1960's,[1–3] but interest has sparked since the demonstration of a DBFC by Amendola *et al.* in 1999.[4] Power densities similar to those attained from direct methanol fuel cells (DMFCs) have been demonstrated, despite substantially less research focus. The lack of effective anode materials for the electrocatalysis of borohydride oxidation is the major limitation in advancing the application of these devices. The complexity of the (up to) eight electron oxidation reaction limits the ability to rationally design a catalytic material towards improved activity or selectivity for key elementary reaction steps. Our group has applied quantum mechanical (*ab initio*) methods to elucidate elementary reaction mechanisms of borohydride oxidation[5,6] and to evaluate novel compositions of binary metal compositions for improved activity. In this perspective, we motivate the use of computational quantum mechanics for this application and illustrate its usefulness in mechanism determination and borohydride oxidation catalyst design.

Numerous recent reviews have discussed the advantages, disadvantages, and state of the art in direct borohydride fuel cells.[7–13] Herein, these are briefly reviewed to provide motivation to the development of more effective borohydride oxidation catalysts. A brief survey of the literature on borohydride oxidation catalysis is provided, highlighting the need for mechanism determination to guide rational catalyst design. A brief description of our approaches for applying quantum chemical methods to electrocatalytic systems is given, and the mechanistic insights provided by this methodology are described. The use of these computational methods to guide the design of binary metal catalysts is discussed in context of the prospective for improved catalyst performance.

Department of Chemical Engineering, Pennsylvania State University, University Park, PA, 16802, USA. E-mail: mjanik@psu.edu; Fax: +1 814 865 7846; Tel: +1 814 863 9366

Broader context

Direct borohydride fuel cells (DBFCs) have the potential to meet power demands for portable electronic applications. DBFCs use an aqueous, base stabilized sodium borohydride solution as the fuel. This fuel has a volumetric energy density approximately half that of gasoline at its solubility limit. DBFC power densities similar to direct methanol fuel cells have been demonstrated despite limited research emphasis. However, the lack of a highly effective anode electrocatalyst for the borohydride oxidation reaction limits the device performance. In this perspective, we review the experimental literature on borohydride oxidation catalysis to motivate the application of computational quantum mechanics for mechanism elucidation and to guide rational design of improved electrocatalysts. Quantum mechanical methods applied to the electrochemical interface provide direct access to elementary reaction energetics at the electrocatalyst surface. The elementary reactions that dictate the relative activity and selectivity of previously tested single-metal catalysts are detailed, and we propose a binary-metal catalyst for improved performance.

2. Direct borohydride fuel cell overview

Direct borohydride fuel cells offer a number of potential advantages over proton exchange membrane fuel cells (PEMFCs) using hydrogen or methanol (direct methanol fuel cells, DMFCs) as an anode fuel. Fig. 1 shows a schematic representation of a direct borohydride fuel cell. DBFCs oxidize an aqueous, base stabilized BH_4^- anion at the anode, producing an environmentally benign, water soluble BO_2^- product which may be collected and recycled. The aqueous fuel offers less storage and handling difficulties than hydrogen, making DBFCs practical for portable power applications. Borohydrides have been extensively studied[14–22] and applied[23–26] for H_2 storage, however, *direct oxidation* has the potential for greater power density and fuel efficiency by minimizing the loss of stored chemical energy through the exothermic H_2 release reaction. The specific energy density of solid sodium borohydride is 9.3 kW h kg^{-1}, approximately 50% greater than pure methanol. The volumetric energy density at the aqueous solubility limit is approximately half that of gasoline. DBFCs with power densities of 200 mW cm^{-2} (with air/oxygen as the oxidant), a value competitive with state-of-the-art DMFCs, have been demonstrated.[27,28] Therefore, DBFCs already offer competitive cell sizes and volumetric fuel consumption rates despite the substantially greater research effort focused on DMFC development. Using hydrogen peroxide as the oxidant, direct borohydride fuel cells can operate without gaseous reactants or products[29–31] and offer power densities as high as 680 mW cm^{-2} at 60 °C. DMFCs and PEMFCs require expensive noble metal cathode catalysts, yet cathode overpotentials still limit device performance. In the DBFC, the alkaline oxygen reduction reaction is catalyzed efficiently by noble metals (Pt,[27,32,33] Ni,[34] and Ag[33–35]) and non-noble electrodes such as MnO_2[36,37] and iron tetramethoxyphenyl porphyrin.[34] The potential of DBFCs is further indicated by their growing research interest. Following Amendola's report in 1999, DBFC related reports in the literature have increased each year

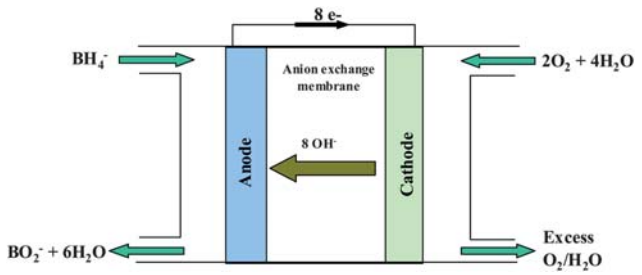

Fig. 1 Schematic of a direct borohydride fuel cell. Aqueous, base stabilized borohydride ions (BH_4^-) are oxidized at the cathode by hydroxide ions to form borate ions (BO_2^-) and water. At the cathode, humidified air or oxygen is reduced to form hydroxide ions, which are transported across an anion conducting membrane to the anode.

Table 1 Advantages and challenges to application of direct borohydride fuel cells

DBFC advantages	DBFC challenges
Aqueous anode fuel	*Borohydride synthesis inefficient*
High gravimetric and volumetric energy density	*Inefficiencies of anode electrocatalysis*
Recyclable BO_2^- product	BH_4^- crossover to cathode[27,32,33,138]
BH_4^- safety and environmental concerns reasonable,[7,139] BO_2^- product benign	Product collection required, accumulation in electrolyte avoided
General AFC concerns	
No anode CO poisoning	Carbonate formation from CO_2[140–143]
Efficient oxygen reduction cathodes with less expensive, non-Pt catalysts[143,144]	Device degradation in basic conditions[140–143]
Demonstrated performance in space[142] and personal transportation applications[141]	Anion transport membranes less developed

Gholamreza Rostamikia

Gholamreza Rostamikia entered Pennsylvania State University as a graduate student in 2006. He received his Bachelor's degree from Amirkabir University of Technology (Tehran Polytechnic) where he graduated in the top 1% of his class in 1998. He also received a Master's degree from Tehran Polytechnic and worked in the oil and gas industry in Iran before joining the Janik research group in January 2007. His research applies computational chemistry to rational design of efficient catalysts for borohydride oxidation reactions.

Michael Janik

Michael Janik joined Penn State as an Assistant Professor of Chemical Engineering in 2006. He received a BS from Yale University in 1998 and PhD from the University of Virginia in 2006, both in Chemical Engineering. His research applies electronic structure methods to a range of catalysis and materials design challenges in energy conversion. Ongoing research projects are in electrocatalysis development for fuel cells, catalysis for hydrogen production, fuel desulfurization, and polymer electrolyte design for battery applications. Janik has authored or co-authored over 30 peer reviewed publications and is currently President of the Pittsburgh-Cleveland Catalysis Society.

from less than 10 per year through 2003 to 35 in 2006, and 71 in 2009.[38]

The main advantages and challenges of direct borohydride fuel cells are summarized in Table 1. Inefficiencies in fuel production and fuel availability limit the widespread applicability of direct borohydride fuel cells. A number of synthesis methods exist,[14,39–47] and this is an active research area due both to the potential of DBFCs and the use of borohydrides for H_2 storage. Large scale use will require recycling of the spent borate product; electrochemical reduction has not been successful in regenerating borohydride,[40] though solid state reactions of sodium metaborate ($NaBO_2$) under gas phase hydrogen have been shown to regenerate solid sodium borohydride.[14,47] Currently, the power densities generated by DBFCs are competitive with DMFCs for small scale portable applications requiring a liquid fuel, however, the direct oxidation efficiency and power density are not competitive with the alternative use of borohydrides for H_2 generation followed by PEMFC conversion. These concerns limit DBFCs to small scale applications that are sensitive to energy density and avoid the indirect process either for device simplification (recharging of portable electronics) or because gas-handling is especially difficult (underwater applications). Inefficiencies associated with borohydride oxidation at the DBFC anode are a major limitation in the performance of DBFCs and must be addressed before further development of this technology may be expected.

3. Borohydride electrooxidation review

Though other losses exist, the majority of deviations in the DBFC operating cell potential from the ideal can be attributed to anode processes. In the DBFC, anode potential losses limit the fuel efficiency to ~30% at practical power densities,[4,9] and the design of effective catalysts is severely challenged by non-selective pathways. Low activity and/or poor selectivity to desired products of anode catalysts are the major factors limiting the performance of DBFCs. Though multiple metals have been demonstrated as potential catalysts for the anode reaction, each has its drawbacks. Nickel,[3,35,48–50] palladium,[49] platinum,[2,48,49,51,52] gold,[4,48,49,52–54] silver,[48,54,55] and hydrogen storage alloys (ZrTiMnVCoNi[27] and LmNiMn[56]) show activity for the anodic oxidation of borohydrides. Each of these suffer from efficiency losses due to deviation from the equilibrium potential and coulombic efficiency losses due to the non-selective hydrolysis of borohydride (Fig. 2). Gold[4,53,54] and silver[54] anodes have been claimed to show the best selectivity to oxidation *versus* hydrolysis, with 7–8 electrons produced per borohydride molecule. However, recent studies have demonstrated that substantial hydrogen gas production can result from Au electrodes,[57–60] with the number of electrons produced per borohydride molecule ranging from ~4 to 7.5 depending on anode potential,[58,60] borohydride concentration,[60] and solution pH.[54] Regardless of coulombic efficiency, slow electrode kinetics limit the power density generated from Au anodes such that substantial potential losses are required to accelerate oxidation and attain a practical power density. Low coulombic efficiencies are typically reported over Group 10 metals, including $4e^-$ per BH_4^- molecule over nickel,[49] 4 to $6e^-$ over palladium[49] and $4e^-$ over platinum.[49] In each case, the remainder of the potential 8 electrons is lost through the production of hydrogen, and the ratio of hydrogen production to current generation increases for higher concentration of borohydride or lower anode overpotentials. Clearly, a complex combination of electrochemical and chemical elementary steps accounts for the direct oxidation and hydrolysis reactions, and differences in the relative energetics of these steps account for the selectivity variations among metals. Mechanistic understanding of the competing reaction paths at the borohydride anode is required for rational anode design to improve selectivity to direct oxidation and increase activity for power generation.

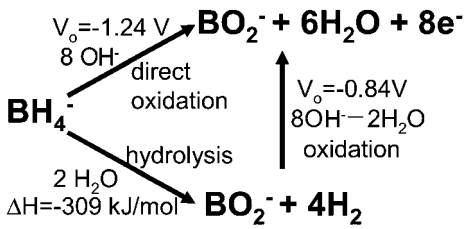

Fig. 2 Hydrolysis of borohydride competes with oxidation, therefore wasting some of the chemical energy stored in the fuel in the exothermic reaction. Subsequent oxidation of the four hydrogen molecules released through hydrolysis produces approximately 25% less electrical energy per original borohydride molecule than direct oxidation. Hydrogen production within the DBFC also represents a coulombic efficiency loss if the hydrogen is released from the cell, as less than 8 electrons are generated per borohydride molecule. Furthermore, the need to separate, transport, and "dispose" of the produced hydrogen would limit the practicality of operating the DBFC.

Despite the multitude of studies testing different noble metal anodes in the DBFC, proposed reaction mechanisms remain rather speculative. A stable BH_3OH^- intermediate is often proposed because it has been identified in the hydrolysis reaction,[61–64] and rotating ring disk electrode studies show an intermediate is produced that can be oxidized at lower potentials than borohydride ions.[59,60] Elder and Hickling proposed an initial $2e^-$ oxidation step on Pt to a stable surface-bound BH_3OH^- species.[2] This initiation step is followed by competitive oxidation and hydrolysis steps. The complete, $8e^-$ oxidation on Au has been proposed to initiate similarly, though Mirkin *et al.*[53] propose that an intermediate monoborane (BH_3) species may leave the Au anode surface and dimerize rather than forming BH_3OH^-. Speculation as to the elementary steps that comprise the overall $8e^-$ reaction is generally limited to the initial reactions, such as a proposed electrochemical–chemical–electrochemical (ECE) sequence for the initiation reaction by Mirkin *et al.*[53] Postulated mechanisms are based entirely on electrokinetic studies of borohydride oxidation (cyclic voltammetry (CV), chronoamperometry, rotating disk electrode (RDE) and rotating ring-disk electrode (RRDE) experiments) that do not provide sufficient information for determination of elementary steps for such a complex reaction. The difficulty of applying interfacial characterization techniques to the aqueous, electrochemical interface is highlighted by the lack of surface bound species characterization *in situ* during borohydride oxidation. To our knowledge, only a single *in situ* infrared adsorption spectroscopy study has attempted characterization of surface species during reaction, however, the sensitivity to surface species with the

methods employed is unclear.[65] Consequently, most proposed mechanisms include multi-electron reactions as opposed to elementary steps, and typically do not explicitly include surface bound species. The lack of elementary mechanism elucidation leaves the role of the catalyst in specific bond breaking or forming reactions unclear, and therefore limits the potential for rational design of improved catalysts.

Quantum mechanical methods are routinely used in heterogeneous catalysis to aid in mechanism determination and to relate catalyst composition and structure to activity and selectivity. Specifically, density functional theory (DFT) has found wide-spread application for examining reactivity over metal and metal-oxide surfaces.[66,67] Proper representation of the length and time scales associated with the electrochemical interface is challenging within a DFT calculation, however, a number of approaches have been developed. The following section provides a brief description of these methods. DFT methods have successfully determined elementary energetics of catalytic reactions relevant to fuel cell electrodes such as oxygen reduction,[68–80] hydrogen oxidation/evolution,[81–83] and methanol/carbon monoxide oxidation.[84–95] We have applied DFT methods to evaluate the reaction mechanism of borohydride oxidation over the Au(111)[5] and Pt(111)[6] surfaces. These results are summarized in context of specific mechanistic questions raised within the borohydride oxidation literature. The prospects for DFT methods to guide the rational design of metal alloys for improved borohydride electrooxidation activity and selectivity are discussed.

4. Density functional theory methods for electrocatalysis

Density functional theory methods can be used to determine the electronic energy of a set of nuclei and electrons. Fig. 3 provides a schematic overview of the application of DFT to catalysis. The

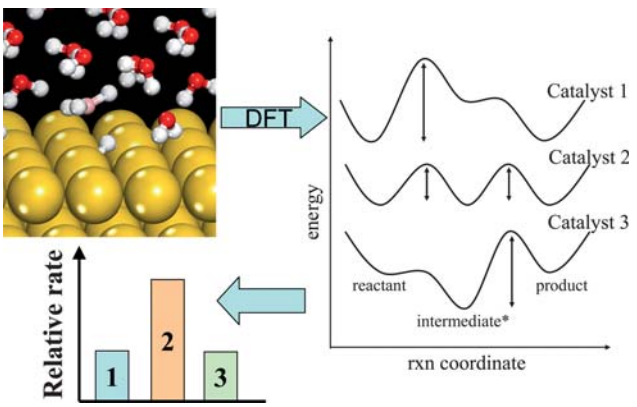

Fig. 3 Schematic overview of the application of DFT methods to catalysis. A model of the catalyst–adsorbate system is created, shown as the transition state for B–H dissociation of BH_4* on the Au(111) surface in the presence of water. DFT methods are used to determine the optimal nuclei arrangement and electronic structure, returning the energy of the system. This is repeated for reactants, intermediates, products, and transition states to construct a reaction energy diagram. Coupled with a kinetic model, the relative rates of a reaction across multiple catalysts can be determined.

electrons and nuclei associated with the catalyst and a reactant, intermediate, or product state of the reaction constitute the model. Optimization methods and DFT algorithms are used to determine the structure and energy of stable states and transition states along a reaction coordinate transforming the reactant to products. These methods can evaluate which intermediates are stable on the catalyst surface, which reaction steps have large and possibly limiting activation barriers, and, together with a kinetic model, the relative rates of reaction over multiple surfaces. In conjunction with experiment, DFT may provide more detailed explanation of observed kinetic behavior, or, because the DFT algorithms are based directly on quantum mechanical principles rather than empirical data, DFT may predict the performance of yet untested catalysts.

The electrocatalytic environment presents challenges to the development of appropriate DFT model systems. Within the fuel cell, the kinetics of oxidation at the anode, ion transport across the membrane, and reduction at the cathode are interdependent, making the initial simplification of the model system to a single metal–adsorbate interface less straightforward than a typical heterogeneous catalytic system. Experimentally, model electrode studies isolate a single working electrode by replacing the complexity of a fuel cell with a simpler electrolyte and a standardized counter electrode. A similar "half-cell" approach can be used in a DFT model, however, complications remain in representing the potential control and electrolyte interactions of the model electrode experiment. The challenge to using DFT methods to determine the elementary reaction energies is in defining a model system that appropriately represents the interactions at a single electrode while also providing for the consideration of elementary processes that involve electrons and ions that begin or complete the reaction step in a different environment. Computational evaluation of electrocatalytic reaction energetics should (a) include the energies of adsorbates (reactants, intermediates, or products, including ions) in the bulk electrolyte prior to adsorption, (b) consider the potential dependence of electrons produced/consumed, and (c) characterize the interaction of adsorbates and transition states with the controlled metal Fermi level and resulting interfacial electrolyte structure when calculating surface reaction energies and activation barriers.

A number of QM model constructions have been developed to probe electrocatalytic reactions. Detailed method comparisons, typically targeted towards an *ab initio* electrochemistry audience, are available;[96–98] here we note the salient features of the specific modeling approaches used to investigate borohydride electrooxidation. The Nørskov[71,84] and Neurock[88,99–102] groups have developed approaches using periodic density functional theory (DFT) to examine the electrocatalytic interface, allowing representation of the extended electronic structure of a metal surface. Proper representation of bulk phase adsorbate energies and electron energies is achieved with either of two approaches. The chemical potential of a hydrogen gas molecule is easily calculated with DFT methods, and its equivalence with the proton–electron pair chemical potential at the normal hydrogen electrode (NHE) potential can be used to give both the proton energy and place the electron energy on the NHE scale.[71] For any species, gas phase chemical potentials can be calculated with DFT and adjusted by the experimental or computational free energy of

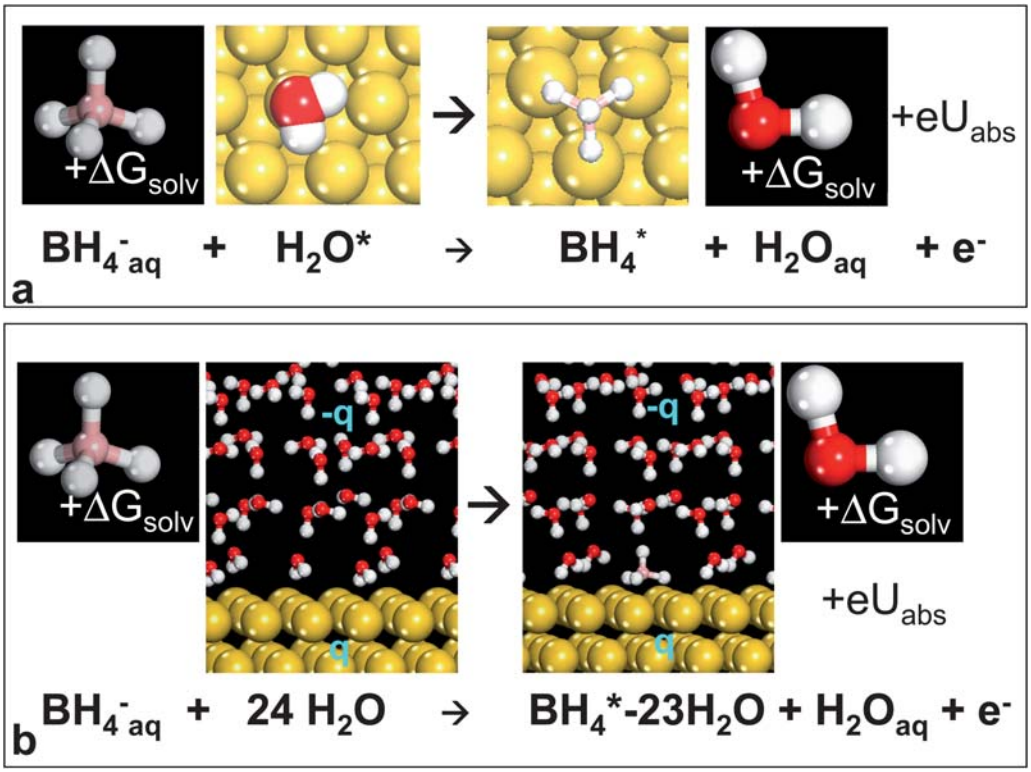

Fig. 4 Density functional theory approaches for calculating the potential dependent adsorption free energy of the BH_4^- ion to the Au(111) surface. (a) The vacuum slab, linear free energy approach considers only the energy of the electron as dependent on the electrode potential through reference to the absolute potential scale (U_{abs}). (b) The double-reference method considers the energy of the $24H_2O$ and BH_4* + $23H_2O$ systems as dependent on electrode potential by directly including a separation of charge q between the metal surface and a homogeneously distributed counter-charge. Explicit water molecules are used to include adsorbate–solvent interactions.

solvation to provide the solution phase chemical potential.[5] With this approach, the electron energy is then used on the absolute/vacuum scale, and corrected to an experimentally accessible (NHE) scale.[103]

Most troublesome in creating an accurate DFT model of the electrochemical interface is representing the interaction of adsorbates with the charged metal surface, counter-ions, and solvent at the electrode–electrolyte interface. The length and time scales associated with the dynamic interfacial structure are not directly accessible due to the computational intensity of DFT methods. Interaction with solvent may be approximated by including a static "microsolvation" of a few (1 to 50) explicit water molecules directly interacting with the adsorbate[71,97,101] or through combining a DFT representation with a continuum solvation model.[98,104] Interaction with the metal-ion separated charge at the interface can be approximated by including an applied external electric field in the simulation,[73] adjusting adsorbate energies for a supposed interfacial dipole–field interaction post-hoc,[71,84,97] or explicitly charging the electrode and prescribing some countercharge distribution[98,101,102,105] or explicitly including charge compensating ions[101,106] within the model system. Our studies of borohydride oxidation have employed the "vacuum slab, linear free energy" approach and the "double-reference method" developed in the Neurock group. The first of these approaches is computationally facile for use in considering a large number of adsorbed species or metal surfaces, but neglects interactions of adsorbates with solvent or electrolyte. This introduces possible error if these interactions differ substantially between adsorbed reactants, intermediates, or products. The second includes a static representation of aqueous solvation at the interface and varies the electrode charge/countercharge to better represent adsorbate energies at the electrochemical interface. This method is computationally intense, and applied only to evaluate the initial borohydride adsorption and dissociation steps. Fig. 4 schematically illustrates the calculation of the borohydride ion adsorption energy with each of these methods.

5. Borohydride oxidation on Au and Pt surfaces

Density functional theory methods have been applied to evaluate the adsorption of the borohydride ion and subsequent transformation of the adsorbed BH_4* species over the Au(111)[5] and Pt(111) species.[6] The reader is referred to these references for a detailed presentation of computational results and the specific DFT approaches used. Herein, these theoretical results are analyzed in context of specific mechanistic questions raised in the experimental borohydride oxidation literature. Prior to this discussion, limitations in the modeling approaches are addressed. These results considered reactions occurring with specific interaction with the catalytic surface, and did not assess the desorption of intermediate species from the surface, the solution phase

reactivity of any desorbed species, or the possibility of electron transfer events occurring without specific binding to the electrode. The experimental literature has clearly demonstrated that the activity of borohydride oxidation is dependent on the catalyst identity, and though there is the possibility of intermediate desorption and solution phase reactions within the complex overall reaction, our intent is to clarify how the relative ability of metals to break or form bonds impacts their catalytic activity. Direct quantitative comparison with experiments over polycrystalline surfaces is also challenged by the computational use of the single crystal (111) surface to represent the electrode. Borohydride electro-oxidation proceeds over relatively large Au and Pt particles (>6 nm).[107] Particles of this size will be dominated by the most stable fcc metal (111) surface, making theoretical consideration of this surface reasonable for comparisons of activity and selectivity among metals. As discussed in the previous section, approximations are necessary in constructing a DFT model of the electrochemical interface, and these approximations introduce error into the calculation of elementary reaction energies and activation barriers. Application to other electrochemical processes has suggested that, quantitatively, these errors allow for calculation of potential dependent reaction energies within plus or minus 0.1 V (for example, for water oxidation over Pt(111),[97] and that qualitative differences between metal surfaces can be well captured.[108]

5.1 Why does oxidation on Pt electrodes occur at a substantially lower overpotential than Au electrodes?

Fig. 5 shows the cascade of elementary surface reactions that occur over the Au(111) surface, with the energetically preferred path noted by red arrows. Relative energies of each surface bound intermediate and calculated activation barriers[109] along the preferred path are given at −0.5 V (NHE). The borohydride oxidation equilibrium potential is −1.24 V (NHE), whereas −0.5 V (NHE) is approximately the potential at which the oxidation rate begins to be measurable within the cyclic voltammogram over Au electrodes.[52] The computational results are in qualitative agreement with experiment in that all elementary oxidation steps are favorable (each has a negative Gibb's free energy change) and all activation barriers reasonable (less than 0.75 eV) at this potential. The final 8 electron product of the surface reaction is $B(OH)_3$*, which may desorb and hydroxylate in solution to form the $B(OH)_4^-$ species, a hydrated form of the borate anion in alkaline solution.

Oxidation (or hydrolysis) of borohydride must result in the breaking of four B–H bonds, and DFT indicates that these bond breaking reactions are activated and relatively slow over the Au(111) surface whereas they are fast over the Pt(111) surface. This relative activity for B–H dissociation is the key factor in determining the relative electrode activity, and explains why CV indicates oxidation over Pt electrodes at an overpotential of approximately 0.3–0.4 V whereas an overpotential of 0.7–0.8 V is required over Au electrodes.[52] Adsorption of the borohydride ion to the Pt(111) surface occurs with dissociation of three B–H bonds, leaving adsorbed H* and BH* species, where "*" denotes an adsorbed species (Fig. 6). This dissociative adsorption of borohydride is favorable over the Pt(111) surface at all potentials above the equilibrium potential, however, the oxidation rate is slow until higher potentials because oxidation of the BH* intermediate species (through formation of BHOH* or B*) is slow. BH* conversion becomes favorable at −0.72 V (NHE), in good agreement with the experimentally observed take-off potential in CV.[52] Over Au(111), molecular adsorption of borohydride is preferred (Fig. 6). The adsorption of the borohydride ion is not favorable on the Au(111) surface until a substantial overpotential is reached, and activation of B–H bonds is slow at low overpotentials.

The DFT results over both Au and Pt suggest that, once all B–H activation steps are favorable, the oxidation reaction proceeds downhill in energy to the final product. This is consistent with a single oxidation process, however, multiple

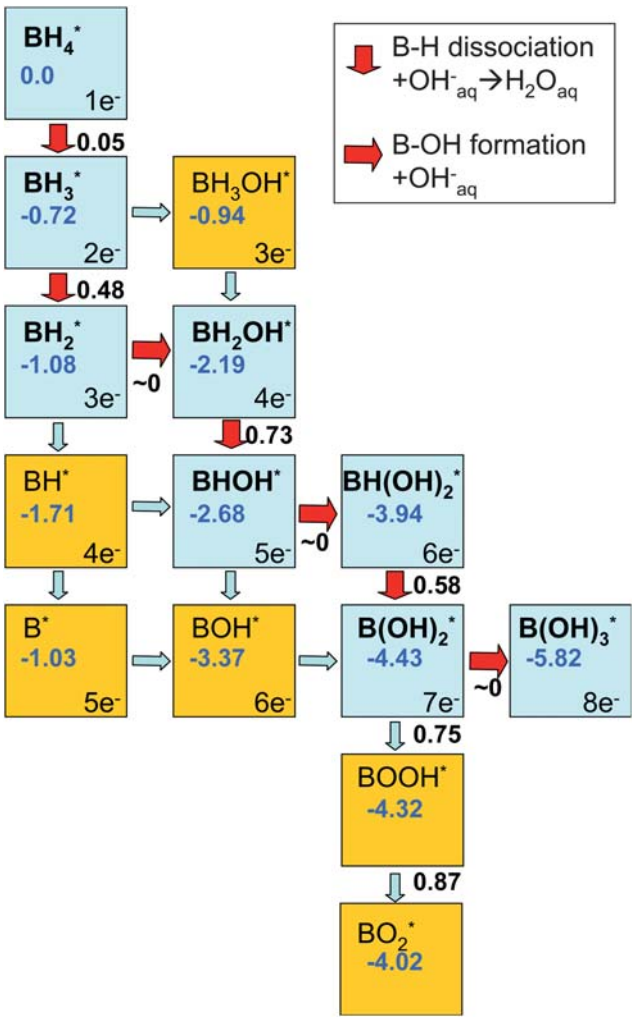

Fig. 5 Reaction path of BH_4* oxidation over the Au(111) surface. The energetically preferred path is given with red (thicker) arrows. Each box is labeled with the chemical identity of the adsorbed intermediate, the energy of the intermediate relative to adsorbed BH_4* at a potential of −0.5 V (NHE), and the number of electrons produced up to that point in the overall reaction. Activation barriers for elementary reactions along the preferred path are given adjacent to reaction arrows. Reaction steps connecting species in columns involve breaking B–H bonds and converting a solution phase hydroxyl anion to a water molecule. Reaction steps along rows form B–OH bonds by adding a solution phase hydroxyl anion to the adsorbed species. All energies are given in eV.

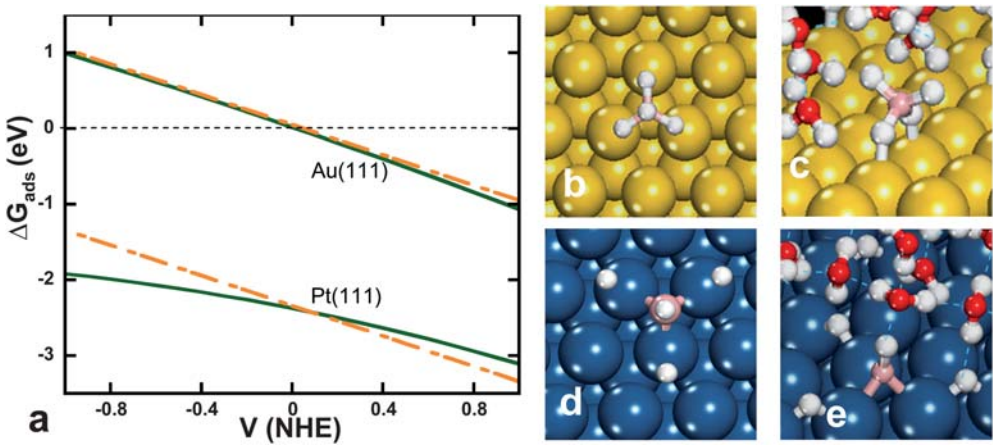

Fig. 6 Structures and adsorption free energy for the borohydride ion to Au(111) and Pt(111) surfaces. (a) Potential dependence adsorption free energy of BH_4^- as a function of electrode potential, calculated as shown schematically in Fig. 4. Dashed lines represent data from the vacuum slab, linear free energy method (Fig. 4a) and solid lines represent data from the double-reference method (Fig. 4b). Chemical potentials were calculated at a temperature of 298 K, BH_4* surface coverage of 1/9 mL, and a solution phase BH_4^- of 0.03 M. Optimized structures of BH_4* adsorbed to the (b and c) Au(111) and (d and e) Pt(111) surface. Adsorption structures were optimized with the (b and d) vacuum slab and (c and e) double-reference models shown at a neutral system charge.

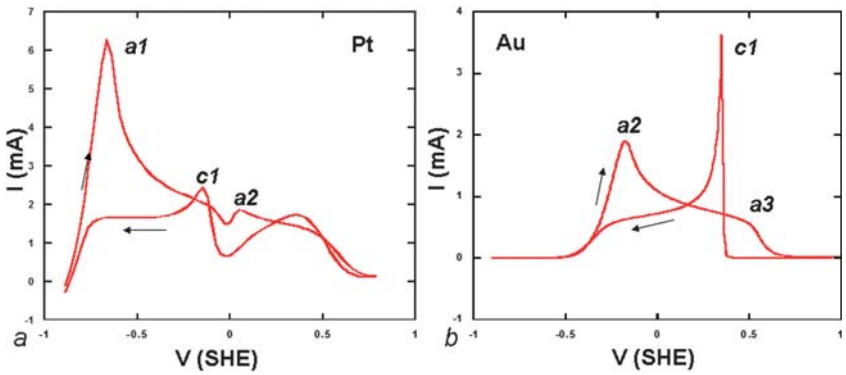

Fig. 7 Cyclic voltammograms for borohydride oxidation over (a) Pt and (b) Au electrodes. Experimental conditions mimic those of Gyenge:[52] $[BH_4^-] = 0.03$ M, $[OH^-] = 2$ M, $T = 295$ K, Au electrode diameter = 3 mm, Pt electrode diameter = 5 mm, and scan rate = 25 mV s^{-1}. Peak labels are following Gyenge.[52]

anodic peaks are typically observed in CV for borohydride oxidation on both Au and Pt electrodes, as illustrated in Fig. 7. On the anodic scan, Pt electrodes (Fig. 7a) show a major peak (*a*1 as noted by Gyenge[52]) at approximately the potential of the reversible hydrogen electrode and a second small peak (*a*2) approximately 0.6 to 0.7 V higher in potential. DFT results suggest that the first peak represents borohydride oxidation, with the competition between hydrogen evolution and oxidation dictated as described in Section 5.2. Though Gyenge speculates the second, *a*2 peak to be indicative of the 8 electron borohydride oxidation reaction, DFT results are not consistent with this explanation. We instead postulate that this second peak is due to formation of surface hydroxide/oxide on platinum, which has been shown to occur approximately 0.6–0.7 V anodic of the reversible hydrogen potential in alkaline media.[110] Similarly, the oxidation peak in the CV cathodic scan (*c*1) may also represent an increase in borohydride oxidation rate as the platinum hydroxide/oxide surface is reduced and the number of active sites for oxidation increased. Au electrodes show a main oxidation peak around −0.2 V (NHE) (Fig. 7b, labeled *a*2 by Gyenge) with a shoulder at +0.4 V (NHE) (*a*3). DFT results are consistent with the lower potential peak representing borohydride oxidation as dissociation of B–H bonds becomes favorable in this potential range. The second *a*3 shoulder again occurs at approximately the potential at which adsorbed hydroxide is formed on Au electrodes,[111,112] suggesting that the decline in current represented by this shoulder is due to hydroxyl groups blocking the surface from further borohydride oxidation. The large oxidation peak observed on the reverse scan (*c*1) occurs as hydroxyl species are reduced from the surface. The surface concentration of borohydride ion is replenished by diffusion during the time the surface is covered in hydroxyl species, providing for the large oxidation current of peak *c*1 once site blocking hydroxyl species are removed. We therefore conclude that the DFT results are not inconsistent with the experimental cyclic voltammogram.

5.2 What determines the selectivity to direct oxidation *versus* hydrolysis?

Though a clear distinction between oxidation and hydrolysis reactions is included in proposed reaction mechanisms,[113,114] the surface elementary steps involved in the two reactions overlap. Adsorption of borohydride on Pt electrodes occurs dissociatively, leaving adsorbed hydrogen on the surface. Activation of B–H bonds is catalyzed by the Au surface, with the resulting H* atoms bound to the surface. Though it is plausible that B–H bond dissociation can occur without resulting in H* adsorbed (equivalent to a Heyrovky *versus* Tafel reaction for H_2 activation[115]), the transition states located thus far with DFT methods[5] suggest direct interaction of the resultant H* product with the metal. The B–H bond activation reactions are not exclusive to the oxidation reaction, and whether these elementary steps result in overall oxidation or hydrolysis reactions depends on the fate of the surface hydrogen produced. If the surface H* coverage resulting from B–H bond activation is greater than that which would be in equilibrium with the gas phase H_2 present, evolution of hydrogen gas will occur through the reaction:

$$H^* + H^* \rightarrow H_{2,gas} + 2^* \quad (1)$$

Oxidation of the adsorbed H* species occurs through:

$$H^* + OH^-{}_{aq} \rightarrow H_2O + * + e^- \quad (2)$$

A higher H* coverage increases the rate of both reactions. Increasing coverage of H* also results in weaker H* adsorption, further increasing evolution and oxidation rates at high coverage. The oxidation reaction also becomes increasingly favorable at more positive electrode potentials. The kinetic competition between these two reactions is, therefore, potential dependent and may also be impacted by mass transfer rates of OH^- or H_2 species to or from the surface. The competition between reactions 1 and 2 will determine whether any surface H* formed results in overall oxidation or hydrolysis reactions. Reaction 1 is second order in H* whereas reaction 2 is first order, indicating higher surface coverages will show greater tendency towards hydrogen evolution.

Significant debate exists in the literature as to whether gold is active for hydrolysis of borohydride.[52,60,116] Au electrodes are typically considered relatively inert for hydrogen oxidation/evolution due to weak binding of H atoms and a low activity for breaking the H–H bond of H_2.[117] For Au electrodes to be active for borohydride oxidation, they must be active for breaking B–H bonds. Evolution of H_2 may then result from any surface H* formed. To begin an analysis of whether H_2 may be expected to evolve, we can neglect the rate of borohydride conversion reactions and calculate the surface coverage of H* that would be in equilibrium with borohydride and borate ions. Surface hydrogen may be generated through the overall reaction:

$$BH_4^-{}_{aq} + 2H_2O_{aq} + 8^* \rightarrow 8H^* + BO_2^-{}_{aq} \quad (3)$$

The chemical potential of the solution phase species was calculated as described previously,[5,6] and the free energy of H* on the Pt(111) and Au(111) surfaces was calculated at coverages of 1/9, 1/3, and 1 monolayer (mL, where 1 mL represents 1 adsorbed H atom per surface metal atom) using the vacuum slab DFT model. The reaction free energy of eqn (3) is then calculated as a function of surface coverage and used to determine the equilibrium coverage of H* given the concentration of the solution phase species. A borohydride solution concentration of 0.03 M is consistent with typical experimental conditions,[52] however, the borate ion concentration is typically undefined. A value of 10^{-6} M was used for the borate ion concentration, consistent with the value used for the "undefined" ion concentration in evaluating dissolution potentials within a Pourbaix diagram.[118] Following this procedure, the equilibrium surface coverage of H* *via* eqn (3) on Au is 0.26 mL and on Pt is 1.00 mL. This is not necessarily the actual H* coverage during oxidation or hydrolysis because we assumed all elementary steps in eqn (3) are fast and neglected reactions 1 and 2 that consume H* species. These high hypothetical coverages simply confirm that both the H* oxidation and evolution reactions are thermodynamically favorable. These coverages represent that which would be in equilibrium with a hydrogen pressure of 1×10^{14} atm (a virtual H_2 pressure,[119,120] calculated considering the equilibrium of eqn (1)) on either metal. As expected from the favorable equilibrium of the evolution reaction, there is a substantial driving force to hydrogen gas evolution if the catalyst is capable of all elementary steps necessary to produce the 8H* species in eqn (3).

Creation of this high hydrogen surface chemical potential requires activity for dissociation of B–H bonds. Four surface hydrogen atoms may be generated from breaking B–H bonds, however, neither Pt or Au has sufficient activity for this at potentials near the borohydride oxidation equilibrium potential (−1.24 V (NHE)). Further reaction of adsorbed BH* on Pt is not favorable until potentials greater than approximately −0.72 V (NHE). At potentials above −0.72 V, all B-containing species can be oxidized from the surface. The combined borohydride oxidation/hydrolysis over Pt electrodes is therefore significantly faster than non-electrochemical hydrolysis because an oxidation overpotential promotes BH* conversion. The combined hydrolysis–oxidation reaction occurs through a combination of B–H bond breaking steps, which may produce H_2 gas or result in oxidation depending on the kinetic competition between eqn (1) and (2), and B–OH bond forming oxidation steps. At low potentials, H* evolution to H_2 gas may outcompete oxidation, resulting in 4 electrons and two molecules of H_2 gas produced per borohydride molecule converted. At higher potentials, oxidation outcompetes with evolution and 8 electrons may be produced per borohydride molecule. Borohydride ion mass transfer limitations may impact the overall rate at high overpotentials, limiting the coverage of H* and therefore further allowing oxidation to compete with evolution. This analysis is consistent with the experimentally observed Pt electrode transition from 4 electrons per borohydride molecule at low current/potential to 8 electrons at high current/potential.[49]

Kinetic limitations to generating a high surface coverage of H* are more severe on Au than Pt, as Au is less effective at breaking B–H bonds. However, at potentials high enough for B–H bond dissociation to be favorable, the same competition between evolution and oxidation of adsorbed H* will dictate the number of electrons produced per borohydride molecule. Therefore, between 4 and 8 electrons may also be expected on Au, in line with the variation observed experimentally.[58,60,116] This analysis also

provides for consideration of how BH_4^- concentration and pH impact the selectivity to direct oxidation. As borohydride concentration is increased, the equilibrium of eqn (3) shifts to the right and a higher coverage of H* may be expected. Higher hydrogen coverage promotes evolution due to the larger reaction order in H* coverage. This is in agreement with the experimental observation that selectivity to direct oxidation over hydrolysis improves for lower borohydride concentrations.[60] A higher hydroxyl concentration will increase the rate of the oxidation reaction (eqn (2)), in agreement with the experimental observation that higher pH results in greater selectivity to direct oxidation.[54]

As the coverage of H* produced is expected to be lower on Au than Pt, Au electrodes are expected to be more selective to direct oxidation than Pt electrodes. Additionally, as B–H dissociation reactions do not become favorable until larger overpotentials, oxidation may be more competitive with evolution when borohydride conversion occurs. Generally, Au electrodes are indicated to be more selective to direct oxidation than Pt electrodes.[8,9] Direct comparison between the theoretical results and a specific electrokinetic experiment is challenging because we have not directly considered the relative rates of eqn (1) and (2) computationally and because the experimental selectivity to direct oxidation may be impacted by relative mass transfer rates and whether the electrode configuration allows for re-adsorption and oxidation of H_2. As any catalyst active for borohydride oxidation must be capable of breaking B–H bonds, improving selectivity to direct oxidation requires increasing the rate of reaction 2 with respect to reaction 1. This may be done by isolating active sites to avoid H–H bond formation, however, this is in conflict with the requirement that the active site be capable of catalyzing multiple B–H dissociation steps. For example, thiourea addition, which is thought to suppress the Tafel process (eqn (1)),[121] reduces the extent of H_2 production over a Pt electrode but also shifts the borohydride oxidation reaction to more positive potentials.[52]

5.3 Could there be a material that catalyzes borohydride oxidation at a potential lower than the reversible hydrogen oxidation potential?

The borohydride oxidation reaction occurs on Pt electrodes at a potential close to the equilibrium potential of hydrogen oxidation (−0.83 V (NHE)), prompting speculation that oxidation must proceed sequentially through gaseous hydrogen production followed by hydrogen oxidation. This may lead to the erroneous conclusion that any catalyst active for hydrogen evolution cannot oxidize borohydride at potentials lower than the standard (1 atm H_2) hydrogen oxidation equilibrium potential. DFT results indicate that borohydride oxidation over Pt cannot occur at potentials lower than −0.85 V due to inactivity for oxidizing adsorbed BH* rather than limitations in oxidizing H_2 gas. Were a catalyst active for all elementary steps oxidizing boron-containing species from the surface, the surface coverage of H* produced would greatly exceed that in equilibrium with 1 atm of H_2, and therefore the equilibrium for oxidation at 1 atm H_2 is not relevant as a limiting potential. The oxidation of this surface bound hydrogen could occur at potentials lower than the standard equilibrium potential at a given pH, and thermodynamic consistency requires that the virtual pressure of H_2 above the catalyst, if all elementary reactions involved in eqn (4) are fast, is equivalent to that at which the equilibrium oxidation potential would be −1.24 V (NHE). Developing a catalyst to be active at potentials below the standard equilibrium potential requires activity for all borohydride oxidation reactions as well as competition of the H* oxidation reaction with evolution.

5.4 Are there stable surface bound intermediates in the borohydride oxidation reaction?

The stable surface bound intermediates of borohydride oxidation likely differ among catalyst materials. Based on DFT calculations, a possible stable intermediate may be identified as a species for which the free energy of production is negative and the subsequent conversion step has a positive free energy or a high activation barrier. Species further along the oxidation reaction coordinate become relatively more stable as the electrode potential becomes more positive, therefore the stability of intermediates may change with potential. On the Pt(111) surface, formation of the BOH* and $B(OH)_2$* species is exoergonic but their subsequent conversion steps are uphill in energy at potentials below approximately −0.8 V (NHE) and the BH* species is stable at potentials below −0.72 V (NHE). Conversions of BOH* and $B(OH)_2$* are only slightly uphill in energy, and as further reaction of these species occurs with small activation barriers and is followed by further exoergonic reactions, neither is likely to achieve a high concentration on the surface. BH* coupling with hydroxyl species to form BHOH* also likely occurs over a low barrier on Pt(111), and as such BH* may only be an observable surface bound intermediate at low potentials. Based on the DFT calculated reaction energy diagram, the elementary reactions may be grouped into kinetically relevant reaction sequences:

$$BH_4^-{}_{aq} + 4* \rightarrow BH* + 3H* + e^- \quad \text{fast, all relevant potentials} \tag{4}$$

$$BH* + OH^-{}_{aq} + * \rightarrow BOH* + H* + e^- \quad \text{slow below } \sim -0.8 \text{ V (NHE)} \tag{5}$$

$$BOH* + 2OH^-{}_{aq} \rightarrow * + B(OH)_3* + 2e^- \quad \text{fast above } \sim -0.9 \text{ V (NHE)} \tag{6}$$

Progress through these reactions determines the overall activity, whereas competition between reactions 1 and 2 determines whether the 4H* species generated in steps 4 and 5 result in oxidation or hydrolysis.

Over the Au(111) surface, the free energy to form BH_3*, BH_2OH*, and $BH(OH)_2$* from an aqueous borohydride ion is negative and the activation barrier to further convert each of these species is greater than 0.40 eV at potentials below −0.3 V (NHE). These species may be observed on the catalyst surface, consistent with the FTIR spectroscopy observation of a B–H related vibrational absorption that shifts with electrode potential.[65] Each of these is also a closed shell molecule in the gas phase. The binding energies of BH_2OH* and $BH(OH)_2$* to the Au(111) surface are less than −0.1 eV, indicating desorption is favored compared to further reaction at all potentials of interest. Their hydroxylated anion forms ($BH_2(OH)_2^-$ and $BH(OH)_3^-$)

may be partial oxidation products. The binding energy of BH_3* to the Au(111) surface is −0.55 eV, indicating that desorption is favored with respect to further oxidation at potentials below −0.67 V (NHE). Desorption of this species from the surface may be expected to form the BH_3OH^- ion in alkaline solution, with selectivity to further oxidation *versus* desorption increasing at more positive potentials. The BH_3OH^- ion has been speculated as an intermediate solution phase product over Au electrodes based on rotating ring-disk electrode experiments.[59,60] Our results indicate that a molecularly adsorbed BH_3OH* is unstable with respect to formation of BOH* and 3H* over the Au(111) surface, and therefore will oxidize at lower potentials than BH_4*. This result is consistent with the experimental observation that BH_3OH^- species generated from NH_3BH_3 decomposition oxidize at a potential ~0.4 V lower than BH_4^- species on Au electrodes.[60,122] Computational results therefore indicate that BH_3OH* may form through surface reactions, however, further dehydrogenation at the surface would be extremely rapid. Solution phase BH_3OH^- may be formed instead through surface generation of BH_3*, which desorbs and is hydroxylated in solution.

6. DFT guided design of borohydride oxidation electrocatalysts

A few encouraging borohydride oxidation studies have demonstrated the ability to modify the performance of noble metal anodes through alloying. A majority of studies investigating binary metal anodes have mixed a metal presumably less active for hydrogen evolution (Ag and Au) with a more active metal (Ir, Pd, Pt, and Ni).[107,123–129] Encouraging results have suggested that the activity of Au or Ag anodes can be improved by adding a metal more active for dehydrogenation (Ir, Pd, or Pt) while also maintaining high coulombic efficiencies.[107,123,124,129] Though these studies are encouraging, the surface composition of the binary metal is typically undefined, the performance of the pure metal catalysts used for comparison often varies substantially between studies, and it is often unclear if the active surface area is maintained constant among catalysts tested in a single study. These results illustrate the potential for alloy design to improve the performance of DBFC anodes, however, the limited testing of alloy performance and the absence of mechanistic insight to drive design leave open the possibility of further advancements. Initial attempts at using DFT methods to predict the kinetic performance of bimetallic catalysts have initiated in our group, and initial results are presented below.

Section 5.1 indicated that the major difference in performance between Au and Pt electrodes is in the activity for breaking B–H bonds. The initial borohydride ion adsorption step (including displacement of a water molecule from the surface)

$$BH_4^-{}_{aq} + H_2O^* \rightarrow BH_4^* + H_2O_{aq} + e^- \quad (7)$$

is used as an initial computational screen for improved borohydride oxidation catalysts. On the Au(111) surface, this initial adsorption is molecular, producing a BH_4* species, and is not favorable until potential near 0 V (NHE). On the Pt(111) surface, adsorption is dissociative, producing BH* + 3H*, and favorable at all relevant potentials. An optimal catalyst will favor molecular adsorption, thereby avoiding establishing a high surface H* coverage that promotes H_2 evolution, while also providing for a stronger adsorption interaction than the Au(111) surface, enabling oxidation activity at lower potentials. Our initial DFT guided alloy design approach is to search for bimetallic surfaces that will offer favorable molecular adsorption at a potential of −0.5 V (NHE). Prior to evaluating bimetallic surfaces, the adsorption free energies of all late transition metal surfaces were evaluated at −0.5 V (NHE). These values are reported in Table 2. Only the Group 11 (Cu, Ag, and Au) surfaces give molecular adsorption, whereas adsorption is dissociative and highly exoergonic on all Group 8–10 metals. At −0.5 V (NHE), adsorption to Au(111) and Ag(111) surfaces is endoergonic, whereas the Cu(111) surface offers molecular and favorable adsorption.

Table 2 The DFT calculated borohydride free energy of adsorption (reaction 7) to late transition metal surfaces at −0.5 V (NHE). 3 × 3 surface cells of the close-packed (111) and (0001) surfaces were used for fcc metals and hcp metals. An "M" indicates that adsorption is molecular, generating a surface BH_4* species, and a "D" indicates that adsorption is dissociative, generating BH* and 3H* species

	Co	**Ni**	**Cu**
	−1.25D	−1.97D	−0.44M
Ru	**Rh**	**Pd**	**Ag**
−1.60D	−1.48D	−2.16D	+ 0.05M
Os	**Ir**	**Pt**	**Au**
−1.85D	−2.01D	−1.85D	+ 0.54M

The calculated adsorption free energy of borohydride adsorption suggests copper electrodes may be ideal for borohydride oxidation. However, copper is not stable with respect to oxidation at a pH of 14 and potentials above −0.4 V (NHE).[130,131] Au–Cu binary metals are more stable to oxidation than pure copper,[132–134] motivating our consideration of Au–Cu surfaces as possible borohydride oxidation catalysts. Fig. 8 illustrates the adsorption geometry for BH_4* on the Au_2Cu_1(111) surface. Adsorption to this surface is molecular with an adsorption free energy of +0.32 eV at −0.5 V (NHE). If this free energy shift carries throughout the oxidation mechanism, a −0.22 V shift to lower potentials is predicted for borohydride oxidation over this Au–Cu surface with respect to pure Au. Realizing the DFT predicted potential shift requires synthesis of a Au–Cu binary metal surface with a similar metal ratio in the surface layer, potentially challenging given the tendency of Au to

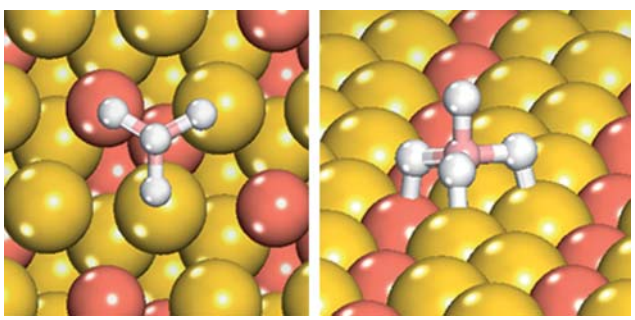

Fig. 8 The structure of BH_4* adsorbed to the Au_2Cu_1(111) surface. Top and profile views are given.

surface segregate in Au–Cu binary mixtures under vacuum.[135] The electrochemical environment may not offer the same surface segregation tendencies, and the synthesis of Au–Cu metal nanoparticles has been demonstrated with surfactant stabilization.[136,137] We are currently pursuing further DFT studies of the complete borohydride oxidation mechanism over Au–Cu surfaces together with experimental electrokinetic studies of Au–Cu electrodes. The mechanistic insight provided by DFT methods will allow for further computational screening of binary metals, and provide new leads for active and selective borohydride oxidation catalysts.

7. Summary

The development of improved borohydride electrooxidation catalysts is necessary for increased borohydride fuel cell application for portable power generation. The complex eight electron oxidation reaction has made experimental mechanism determination difficult, motivating the use of DFT methods for mechanism elucidation and design of improved oxidation catalysts. The application of DFT methods to the electrochemical environment is challenged by the length and time scales associated with solvation and double-layer structure. Recent advances have provided a number of DFT based approaches that allow for electrocatalytic mechanism evaluation and electrode design. Our group has applied DFT methods to the borohydride oxidation mechanism over Pt(111) and Au(111) surfaces. Specific conclusions reached based on DFT results include: (1) the activity for B–H dissociation reactions dictates the relative catalyst activity and (2) the relative rates of surface hydrogen evolving as H_2 gas or oxidizing from the surface determine the overall selectivity to hydrolysis or oxidation. An optimal catalyst will offer higher activity for B–H bond dissociation than Au electrodes together with higher selectivity to oxidation of surface H* than offered by Pt electrodes. DFT methods were used to predict that a Au_2Cu_1(111) surface will oxidize borohydride at an overpotential approximately 0.2 V lower than a pure Au(111) surface. Rational design of binary metal surfaces, based on mechanistic insight obtained *via* quantum chemical methods, may lead to improved catalyst compositions that increase the fuel efficiency and power density of direct borohydride fuel cells.

Acknowledgements

Michael Hickner (Penn State Dept. of Materials Science and Engineering) is acknowledged for help in obtaining the cyclic voltammograms of Fig. 7.

References

1 J. P. Elder, *Electrochim. Acta*, 1962, **7**, 417–426.
2 J. P. Elder and A. Hickling, *Trans. Faraday Soc.*, 1962, **58**, 1852–1864.
3 M. E. Indig and R. N. Snyder, *J. Electrochem. Soc.*, 1962, **109**, 1104–1106.
4 S. C. Amendola, P. Onnerud, M. T. Kelly, P. J. Petillo, S. L. Sharp-Goldman and M. Binder, *J. Power Sources*, 1999, **84**, 130–133.
5 G. Rostamikia and M. J. Janik, *J. Electrochem. Soc.*, 2009, **156**, B86.
6 G. Rostamikia and M. J. Janik, *Electrochim. Acta*, 2010, **55**, 1175–1183.
7 U. B. Demirci, *J. Power Sources*, 2007, **169**, 239–246.
8 U. B. Demirci, *J. Power Sources*, 2007, **172**, 676–687.
9 C. P. de Leon, F. C. Walsh, D. Pletcher, D. J. Browning and J. B. Lakeman, *J. Power Sources*, 2006, **155**, 172–181, .
10 B. H. Liu and Z. P. Li, *J. Power Sources*, 2009, **187**, 291–297.
11 J. Ma, N. A. Choudhury and Y. Sahai, *Renewable Sustainable Energy Rev.*, 2010, **14**, 183–199.
12 J.-H. Wee, *J. Power Sources*, 2006, **161**, 1–10.
13 J.-H. Wee, *J. Power Sources*, 2006, **155**, 329–339.
14 Y. Kojima, K. Suzuki and Y. Kawai, *J. Power Sources*, 2006, **155**, 325–328.
15 B. S. Richardson, J. F. Birdwell, F. G. Pin, J. F. Jansen and R. F. Lind, *J. Power Sources*, 2005, **145**, 21–29.
16 Q. Ge, *J. Phys. Chem. A*, 2004, **108**, 8682–8690.
17 T. J. Frankcombe, G. Kroes and A. Zuttel, *Chem. Phys. Lett.*, 2005, **405**, 73–78.
18 S. Orimo, Y. Nakamori and A. Zuttel, *Mater. Sci. Eng., B*, 2004, **108**, 51–53.
19 K. Miwa, N. Ohba, S. Towata, Y. Nakamori and S. Orimo, *Phys. Rev. B: Condens. Matter*, 2004, **69**, 245120.
20 D. Hua, Y. Hanxi, A. Xinping and C. Chuansin, *Int. J. Hydrogen Energy*, 2003, **28**, 1095–1100.
21 A. Zuttel, P. Wenger, S. Rentsch, P. Sudan, P. Mauron and C. Emmenegger, *J. Power Sources*, 2003, **118**, 1–7.
22 B. Sakintuna, F. Lamari-Darkrim and M. Hirscher, *Int. J. Hydrogen Energy*, 2007, **32**, 1121–1140.
23 S. C. Amendola, S. L. Sharp-Goldman, M. S. Janjua, N. C. Spencer, M. T. Kelly, P. J. Petillo and M. Binder, *Int. J. Hydrogen Energy*, 2000, **25**, 969–975.
24 D. Gervasio, S. Tasic and F. Zenhausern, *J. Power Sources*, 2005, **149**, 15–21.
25 S. W. Jorgensen and B. K. Perry, *US Pat.*, 6 811 764, 2002.
26 S. C. Amendola, P. J. Petillo and S. C. Petillo, *US Pat.*, 2004/0009379, 2004.
27 Z. P. Li, B. H. Liu, K. Arai and S. Suda, *J. Electrochem. Soc.*, 2003, **150**, A868–A872.
28 Z. P. Li, B. H. Liu, K. Arai and S. Suda, *J. Alloys Compd.*, 2005, **404–406**, 648–652.
29 D. X. Cao, D. D. Chen, J. Lan and G. L. Wang, *J. Power Sources*, 2009, **190**, 346–350.
30 L. F. Gu, N. Luo and G. H. Miley, *J. Power Sources*, 2007, **173**, 77–85.
31 G. H. Miley, N. Luo, J. Mather, R. Burton, G. Hawkins, L. F. Gu, E. Byrd, R. Gimlin, P. J. Shrestha, G. Benavides, J. Laystrom and D. Carroll, *J. Power Sources*, 2007, **165**, 509–516.
32 Z. P. Li, B. H. Liu, K. Arai, K. Asaba and S. Suda, *J. Power Sources*, 2004, **126**, 28–33.
33 B. Liu and S. Suda, *J. Power Sources*, 2007, **164**, 100–104.
34 H. Cheng and K. Scott, *J. Electroanal. Chem.*, 2006, **596**, 117–123.
35 B. H. Liu, Z. P. Li, K. Arai and S. Suda, *Electrochim. Acta*, 2005, **50**, 3719–3725.
36 R. X. Feng, H. Dong, Y. D. Wang, X. P. Ai, Y. L. Cao and H. X. Yang, *Electrochem. Commun.*, 2005, **7**, 449–452.
37 Y. Wang and Y. Xia, *Electrochem. Commun.*, 2006, **8**, 1775–1778.
38 Determined using Web of Science with search criteria for "DBFC" or "borohydride fuel cell".
39 S. Suda, N. Morigasaki, Y. Iwase and Z. P. Li, *J. Alloys Compd.*, 2005, **404–406**, 643–647.
40 E. L. Gyenge and C. W. Oloman, *J. Appl. Electrochem.*, 1998, **28**, 1147–1151.
41 Z. P. Li, N. Morigazaki, B. H. Liu and S. Suda, *J. Alloys Compd.*, 2003, **349**, 232–236.
42 Z. P. Li, B. H. Liu, N. Morigasaki and S. Suda, *J. Alloys Compd.*, 2003, **354**, 243–247.
43 D. L. Calabretta and B. R. Davis, *J. Power Sources*, 2007, **164**, 782–791.
44 J. V. Ortega, Y. Wu, S. C. Amendola and M. T. Kelly, *US Pat.*, application 2003/0114632, 2003.
45 S. C. Amendola, M. T. Kelly, J. V. Ortega and Y. Wu, *US Pat.*, application 2003/0092877, 2003.
46 S. C. Amendola and M. T. Kelly, *US Pat.*, 7 019 105, 2006.
47 B. H. Liu, Z. P. Li and J. K. Zhu, *J. Alloys Compd.*, 2009, **476**, L16–L20.
48 H. Cheng, K. Scott and K. Lovell, *Fuel Cells*, 2006, **6**, 367–375.
49 B. H. Liu, Z. P. Li and S. Suda, *Electrochim. Acta*, 2004, **49**, 3097–3105.

50 B. H. Liu, Z. P. Li and S. Suda, *J. Electrochem. Soc.*, 2003, **150**, A398–A402.
51 A. Verma and S. Basu, *J. Power Sources*, 2005, **145**, 282–285.
52 E. Gyenge, *Electrochim. Acta*, 2004, **49**, 965–978.
53 M. V. Mirkin, H. Yang and A. J. Bard, *J. Electrochem. Soc.*, 1992, **139**, 2212–2217.
54 M. Chatenet, F. Micoud, I. Roche and E. Chatinet, *Electrochim. Acta*, 2006, **51**, 5459–5467.
55 E. Sanli, H. Celikkan, B. Z. Uysal and M. L. Aksu, *Int. J. Hydrogen Energy*, 2006, **31**, 1920–1924.
56 L. Wang, C. Ma, Y. Sun and S. Suda, *J. Alloys Compd.*, 2005, **391**, 318–322.
57 M. Chatenet, M. B. Molina-Concha and J. P. Diard, *Electrochim. Acta*, 2009, **54**, 1687–1693.
58 D. A. Finkelstein, N. Da Mota, J. L. Cohen and H. D. Abruna, *J. Phys. Chem. C*, 2009, **113**, 19700–19712.
59 P. Krishnan, T.-H. Yang, S. G. Advani and A. J. Prasad, *J. Power Sources*, 2008, **182**, 106–111.
60 M. Chatenet, F. H. B. Lima and E. A. Ticianelli, *J. Electrochem. Soc.*, 2010, **157**, B697–B704.
61 V. J. Goubeau and H. Kallfass, *Z. Anorg. Allg. Chem.*, 1959, **299**, 160–169.
62 R. E. Davis and C. G. Swain, *J. Am. Chem. Soc.*, 1960, **82**, 5949–5950.
63 J. A. Gardiner and J. W. Collat, *J. Am. Chem. Soc.*, 1964, **86**, 3165–3166.
64 J. A. Gardiner and J. W. Collat, *J. Am. Chem. Soc.*, 1965, **87**, 1692–1700.
65 B. M. Concha, M. Chatenet, C. Coutanceau and F. Hahn, *Electrochem. Commun.*, 2009, **11**, 223–226.
66 M. Neurock, S. A. Wasileski and D. Mei, *Chem. Eng. Sci.*, 2004, **59**, 4703–4714.
67 R. A. v. Santen and M. Neurock, *Molecular Heterogeneous Catalysis: a Conceptual and Computational Approach*, Wiley-VCH, Weinheim, Germany, 2006.
68 J. Zhang, M. B. Vukmirovic, K. Sasaki, A. U. Nilekar, M. Mavrikakis and R. R. Adzic, *J. Am. Chem. Soc.*, 2005, **127**, 12480–12481.
69 J. Zhang, M. B. Vukmirovic, Y. Xu, M. Mavrikakis and R. R. Adzic, *Angew. Chem., Int. Ed.*, 2005, **44**, 2132–2135.
70 J. Greeley and J. K. Nørskov, *Surf. Sci.*, 2005, **592**, 104–111.
71 J. K. Nørskov, J. Rossmeisl, A. Logadottir, L. Lindqvist, J. R. Kitchin, T. Bligaard and H. Jonsson, *J. Phys. Chem. B*, 2004, **108**, 17886–17892.
72 Y. Xu, A. V. Ruban and M. Mavrikakis, *J. Am. Chem. Soc.*, 2004, **126**, 4717–4725.
73 M. P. Hyman and J. W. Medlin, *J. Phys. Chem. B*, 2006, **110**, 15338–15344.
74 T. Li and P. B. Balbuena, *J. Phys. Chem. B*, 2001, **105**, 9943–9952.
75 T. Li and P. B. Balbuena, *Chem. Phys. Lett.*, 2003, **367**, 439–447.
76 A. Panchenko, M. T. M. Koper, T. E. Shubina, S. J. Mitchell and E. Roduner, *J. Electrochem. Soc.*, 2004, **151**, A2016–A2027.
77 J. Greeley and J. K. Nørskov, *J. Phys. Chem. C*, 2009, **113**, 4932–4939.
78 M. J. Janik, C. D. Taylor and M. Neurock, *J. Electrochem. Soc.*, 2009, **156**, B126–B135.
79 K. Y. Yeh, S. A. Wasileski and M. J. Janik, *Phys. Chem. Chem. Phys.*, 2009, **11**, 10108–10117.
80 J. Greeley, I. E. L. Stephens, A. S. Bondarenko, T. P. Johansson, H. A. Hansen, T. F. Jaramillo, J. Rossmeisl, I. Chorkendorff and J. K. Nørskov, *Nat. Chem.*, 2009, **1**, 552–556.
81 J. Greeley and J. K. Nørskov, *Surf. Sci.*, 2007, **601**, 1590–1598.
82 J. Greeley, J. K. Nørskov, L. A. Kibler, A. M. El-Aziz and D. M. Kolb, *ChemPhysChem*, 2006, **7**, 1032–1035.
83 J. Greeley, T. F. Jaramillo, J. Bonde, I. Chorkendorff and J. K. Nørskov, *Nat. Mater.*, 2006, **5**, 909–913.
84 P. Liu, A. Logadottir and J. K. Nørskov, *Electrochim. Acta*, 2003, **48**, 3731–3742.
85 S. Desai and M. Neurock, *Electrochim. Acta*, 2003, **48**, 3759–3773.
86 S. K. Desai and M. Neurock, *Phys. Rev. B: Condens. Matter*, 2003, **68**, 075420.
87 Q. Ge, S. Desai, M. Neurock and K. Kourtakis, *J. Phys. Chem. B*, 2001, **105**, 9533–9536.
88 D. Cao, G.-Q. Lu, A. Wieckowski, S. A. Wasileski and M. Neurock, *J. Phys. Chem. B*, 2005, **109**, 11622–11633.
89 C. Hartnig and E. Spohr, *Chem. Phys.*, 2005, **319**, 185–191.
90 M. T. M. Koper, N. P. Lebedeva and C. G. M. Hermse, *Faraday Discuss.*, 2002, **121**, 301–311.
91 T. E. Shubina, C. Hartnig and M. T. M. Koper, *Phys. Chem. Chem. Phys.*, 2004, **6**, 4215–4221.
92 T. E. Shubina and M. T. M. Koper, *Electrochim. Acta*, 2002, **47**, 3621–3628.
93 T. R. Mattson and S. J. Paddison, *Surf. Sci.*, 2003, **544**, L697–L702.
94 P. Ferrin, A. U. Nilekar, J. Greeley, M. Mavrikakis and J. Rossmeisl, *Surf. Sci.*, 2008, **602**, 3424–3431.
95 M. J. Janik and M. Neurock, *Electrochim. Acta*, 2007, **52**, 5517–5528.
96 M. J. Janik, C. D. Taylor and M. Neurock, *Top. Catal.*, 2007, **46**, 306–319.
97 J. Rossmeisl, J. K. Nørskov, C. D. Taylor, M. J. Janik and M. Neurock, *J. Phys. Chem. B*, 2006, **110**, 21833–21839.
98 R. Jinnouchi and A. B. Anderson, *Phys. Rev. B: Condens. Matter*, 2008, **77**, 245417.
99 C. D. Taylor, R. G. Kelly and M. Neurock, *J. Electrochem. Soc.*, 2007, **154**, F55–F64.
100 C. D. Taylor and M. Neurock, *Curr. Opin. Solid State Mater. Sci.*, 2005, **9**, 49–65.
101 C. D. Taylor, S. A. Wasileski, J. S. Filhol and M. Neurock, *Phys. Rev. B: Condens. Matter*, 2006, **73**, 165402.
102 J. S. Filhol and M. Neurock, *Angew. Chem., Int. Ed.*, 2006, **45**, 402–406.
103 H. Reiss and A. Heller, *J. Phys. Chem.*, 1985, **89**, 4207–4213.
104 M. Otani and O. Sugino, *Phys. Rev. B: Condens. Matter*, 2006, **73**, 115407.
105 A. Y. Lozovoi, A. Alavi, J. Kohanoff and R. M. Lynden-Bell, *J. Chem. Phys.*, 2001, **115**, 1661–1669.
106 J. Rossmeisl, E. Skulason, M. E. Bjorketun, V. Tripkovic and J. K. Nørskov, *Chem. Phys. Lett.*, 2008, **466**, 68–71.
107 M. H. Atwan, C. L. B. Macdonald, D. O. Northwood and E. L. Gyenge, *J. Power Sources*, 2006, **158**, 36–44.
108 C. D. Taylor, M. J. Janik, M. Neurock and R. G. Kelly, *Mol. Simul.*, 2006, **33**, 15–30.
109 G. Rostamikia, A. Mendoza, M. A. Hickner and M. J. Janik, in preparation.
110 N. M. Markovic, H. A. Gasteiger and P. N. Ross, *J. Phys. Chem.*, 1996, **100**, 6715–6721.
111 A. Chen and J. Lipkowski, *J. Phys. Chem. B*, 1999, **103**, 682–691.
112 D. W. Kirk, F. R. Foulkes and W. F. Graydon, *J. Electrochem. Soc.*, 1980, **127**, 1069–1076.
113 J. H. Morris, H. J. Gysling and D. Reed, *Chem. Rev.*, 1985, **85**, 51–76.
114 H. Dong, R. X. Feng, X. P. Ai, Y. L. Cao, H. X. Yang and C. S. Cha, *J. Phys. Chem. B*, 2005, **109**, 10896–10901.
115 N. M. Markovic, B. N. Grgur and P. N. Ross, *J. Phys. Chem. B*, 1997, **101**, 5405–5413.
116 M. Chatenet, M. B. Molina-Concha, N. El-Kissi, G. Parrour and J. P. Diard, *Electrochim. Acta*, 2009, **54**, 4426–4435.
117 B. E. Conway and G. Jerkiewicz, *Solid State Ionics*, 2002, **150**, 93–103.
118 G. A. Prentice, *Electrochemical Engineering Principles*, Prentice-Hall, Inc., Upper Saddle River, NJ, 1991.
119 M. Boudart, *Catal. Lett.*, 1989, **3**, 111–116.
120 E. Iglesia, J. E. Baumgartner and G. L. Price, *J. Catal.*, 1992, **134**, 549–571.
121 T. Maoka and M. Enyo, *Surf. Technol.*, 1979, **9**, 147–157.
122 L. C. Nagle and J. F. Rohan, *J. Electrochem. Soc.*, 2006, **153**, C773–C776.
123 E. Gyenge, M. Atwan and D. Northwood, *J. Electrochem. Soc.*, 2006, **153**, A150–A158.
124 M. H. Atwan, D. O. Northwood and E. L. Gyenge, *Int. J. Hydrogen Energy*, 2007, **32**, 3116–3125.
125 B. M. Concha and M. Chatenet, *Electrochim. Acta*, 2009, **54**, 6119–6129.
126 B. M. Concha and M. Chatenet, *Electrochim. Acta*, 2009, **54**, 6130–6139.
127 M. Simoes, S. Baranton and C. Coutanceau, *J. Phys. Chem. C*, 2009, **113**, 13369–13376.
128 X. Y. Geng, H. M. Zhang, Y. W. Ma and H. X. Zhong, *J. Power Sources*, 2010, **195**, 1583–1588.

129 H. M. Lee, S. Y. Park, K. T. Park, U. H. Jung, K. Chun, C. D. Woong and S. H. Kim, *Res. Chem. Intermed.*, 2008, **34**, 787–792.
130 M. Pourbaix, *Atlas of Electrochemical Equilibria in Aqueous Solutions*, NACE, Houston, TX, 1974.
131 M. Ziomek-Moroz, A. Miller, J. Hawk, K. Cadien and D. Y. Li, *Wear*, 2003, **255**, 869–874.
132 B. G. Ateya, G. Geh, A. H. Carim and H. W. Pickering, *J. Electrochem. Soc.*, 2002, **149**, B27–B33.
133 G. S. Duffo, S. B. Farina and J. R. Galvele, *Corros.Sci.*, 2004, **46**, 1–4.
134 J. D. Fritz and H. W. Pickering, *J. Electrochem. Soc.*, 1991, **138**, 3209–3218.
135 A. V. Ruban, H. L. Skriver and J. K. Nørskov, *Phys. Rev. B: Condens. Matter*, 1999, **59**, 15990–16600.
136 A. K. Sra, T. D. Ewers and R. E. Schaak, *Chem. Mater.*, 2005, **17**, 758–766.
137 A. K. Sra and R. E. Schaak, *J. Am. Chem. Soc.*, 2004, **126**, 6667–6672.
138 H. Cheng, K. Scott, K. V. Lovell, J. A. Horsfall and S. C. Waring, *J. Membr. Sci.*, 2007, **288**, 168–174.
139 Safety concerns are reasonable based on the Materials Safety Data Sheet, accessed from the Sigma-Aldrich website (www.sigmaaldrich.com) on May 31, 2010.
140 E. Gulzow, *J. Power Sources*, 1996, **61**, 99–104.
141 K. Kordesch, V. Hacker, J. Gsellmann, M. Cifrain, G. Faleschini, P. Enziger, R. Fankhauser, M. Ortner, M. Muhr and R. R. Aronson, *J. Power Sources*, 2000, **86**, 162–165.
142 M. Cifrain and K. V. Kordesch, *J. Power Sources*, 2004, **127**, 234–242.
143 G. F. McLean, T. Niet, S. Prince-Richard and N. Djilali, *Int. J. Hydrogen Energy*, 2002, **27**, 507–526.
144 B. Y. S. Lin, D. W. Kirk and S. J. Thorpe, *J. Power Sources*, 2006, **161**, 474–483.

